JOURNAL OF GEOPHYSICAL RESEARCH, VOL. 116, D09203, doi:10.1029/2010JD015274, 2011

Global distribution of cloud droplet number concentration, autoconversion rate, and aerosol indirect effect under diabatic droplet activation

Donifan Barahona,[1,2] Rafaella Sotiropoulou,[3,4] and Athanasios Nenes[1,3]

Received 9 November 2010; revised 11 February 2011; accepted 15 February 2011; published 7 May 2011.

[1] This study presents a global assessment of the sensitivity of droplet number to diabatic activation (i.e., including effects from entrainment of dry air) and its first-order tendency on indirect forcing and autoconversion. Simulations were carried out with the NASA Global Modeling Initiative (GMI) atmospheric and transport model using climatological metereorological fields derived from the former NASA Data Assimilation Office (DAO), the NASA Finite volume GCM (FVGCM) and the Goddard Institute for Space Studies version II' (GISS) GCM. Cloud droplet number concentration (CDNC) is calculated using a physically based prognostic parameterization that explicitly includes entrainment effects on droplet formation. Diabatic activation results in lower CDNC, compared to adiabatic treatment of the process. The largest decrease in CDNC (by up to 75%) was found in the tropics and in zones of moderate CCN concentration. This leads to a global mean effective radius increase between 0.2–0.5 μm (up to 3.5 μm over the tropics), a global mean autoconversion rate increase by a factor of 1.1 to 1.7 (up to a factor of 4 in the tropics), and a 0.2–0.4 W m^{-2} decrease in indirect forcing. The spatial patterns of entrainment effects on droplet activation tend to reduce biases in effective radius (particularly in the tropics) when compared to satellite retrievals. Considering the diabatic nature of ambient clouds, entrainment effects on CDNC need to be considered in GCM studies of the aerosol indirect effect.

Citation: Barahona, D., R. Sotiropoulou, and A. Nenes (2011), Global distribution of cloud droplet number concentration, autoconversion rate, and aerosol indirect effect under diabatic droplet activation, *J. Geophys. Res.*, *116*, D09203, doi:10.1029/2010JD015274.

1. Introduction

[2] Cloud droplet number concentration (CDNC) depends on the size distribution and composition of the precursor aerosol, and, on the thermodynamical and dynamical (i.e., updraft velocity, mixing rates) state of the cloudy air during its formation [*Seinfeld and Pandis*, 1998]. Increasing the precursor aerosol number concentration may lead to a decrease in cloud effective radius and therefore to an increase in cloud albedo, i.e., the first aerosol indirect effect [*Twomey*, 1977]. The limited ability of general circulation models (GCMs) to explicitly represent aerosol-cloud interactions motivated the development of physically based representations parameterizations of the cloud droplet formation process [*Abdul-Razzak and Ghan*, 2000; *Nenes and Seinfeld*, 2003; *Fountoukis and Nenes*, 2005; *Ming et al.*, 2006; *Kumar et al.*, 2009]. State-of-the-art parameterizations take into account effects of the aerosol composition, such as the role of organic surfactants and solutes [*Fountoukis and Nenes*, 2005; *Abdul-Razzak and Ghan*, 2005], adsorption activation [*Kumar et al.*, 2009], and kinetic and mass transfer limitations on droplet formation [*Fountoukis and Nenes*, 2005; *Asa-Awuku and Nenes*, 2007; *Barahona et al.*, 2010], and mixing and entrainment [*Barahona and Nenes*, 2007].

[3] State-of-the-art atmospheric models use double-moment cloud microphysics schemes (which vary significantly in how each cloud moment is computed), in which the time evolution of the moments of the droplet size distribution is determined by grid-scale advection, detrainment, turbulent diffusion, and microphysical processes [e.g., *Takemura et al.*, 2005; *Quaas et al.*, 2009; *Chen et al.*, 2010; *Ghan et al.*, 1997; *Lohmann and Feichter*, 1997; *Morrison and Gettelman*, 2008]. The calculated total liquid condensate mass (LWC) and the cloud droplet number concentration (CDNC) are then used to estimate the cloud optical properties

[1]School of Chemical and Biomolecular Engineering, Georgia Institute of Technology, Atlanta, Georgia, USA.
[2]Now at Global Modeling and Assimilation Office, NASA Goddard Space Flight Center, Greenbelt, Maryland, USA.
[3]School of Earth and Atmospheric Sciences, Georgia Institute of Technology, Atlanta, Georgia, USA.
[4]Environmental Research Laboratory, Demokritos National Center of Scientific Research, Aghia Paraskevi, Greece.

0148-0227/11/2010JD015274

(e.g., droplet effective radius, R_{eff}, and optical depth) and autoconversion rate. In these schemes cloud condensation nuclei (CCN) activation represents a source of cloud droplets. CCN activation is typically parameterized considering the adiabatic ascent of air parcels from cloud base [e.g., *Abdul-Razzak and Ghan*, 2000; *Fountoukis and Nenes*, 2005; *Ming et al.*, 2006; *Segal and Khain*, 2006]. It is, however, well known that real clouds are predominantly subadiabatic; field observations show both CDNC and LWC below the adiabatic limit, which results from mixing and entrainment of dry air throughout the cloud lifetime [*Brenguier and Chaumat*, 2001; *Conant et al.*, 2004; *Lu et al.*, 2008; *Pruppacher and Klett*, 1997].

[4] Mixing and entrainment of environmental air affects cloud formation over multiple spatial scales. Radiatively induced turbulent mixing near cloud top may trigger the breakup and dissipation of stratocumulus decks [e.g., *Bretherton et al.*, 2004; *Stevens*, 2005; *Gerber et al.*, 2005]. Lateral entrainment weakens updrafts affecting the formation of cumulus and deep convective clouds [e.g., *Carpenter et al.*, 1998; *Chosson et al.*, 2007; *Cohen*, 2000; *Lin and Arakawa*, 1997; *Rogers et al.*, 1985; *Stommel*, 1947]. The microphysics of cloud formation is also affected by entrainment as it modifies the drop size distribution [e.g., *Pruppacher and Lee*, 1976; *Paluch*, 1979; *Raga et al.*, 1990; *Raga and Jonas*, 1993; *Cohen*, 2000; *Neggers et al.*, 2003; *Barahona and Nenes*, 2007; *Lu et al.*, 2008]; neglecting entrainment effects on CDNC (the current assumption in GCMs) produces much more narrow droplet size distributions when compared to observations [e.g. *Lin and Arakawa*, 1997; *Cohen*, 2000; *Brenguier and Chaumat*, 2001; *Snider et al.*, 2003; *Morrison and Grabowski*, 2008; *Pruppacher and Klett*, 1997; *Hsieh et al.*, 2009b].

[5] GCM cloud schemes account implicitly for entrainment and mixing effects on liquid condensate by introducing empirically derived subgrid probability distributions of LWC or by prescribing the LWC vertical profile as a function of the large-scale temperature and relative humidity fields [e.g., *Takemura et al.*, 2005; *Quaas et al.*, 2009; *Chen et al.*, 2010; *Ghan et al.*, 1997; *Lohmann and Feichter*, 1997; *Morrison and Gettelman*, 2008; *Hack*, 1998]. However, the CDNC vertical profile is often still assumed equal to the upper limit of adiabatic activation (Figure 1b). This treatment is inherently inconsistent, with a tendency for overestimating CDNC and underestimating droplet size, with important implications for indirect effect assessments [e.g., *Kim et al.* 2008].

[6] The assumption of adiabatic activation stems from considering droplet formation in large-scale clouds as occurring solely within the core of horizontally homogeneous stratocumulus decks; this approach, however, leaves out the very common trade wind cumulus of the tropical regions [*Albrecht et al.*, 1995]. Furthermore, it is known that in tropical and subtropical marine environments cumulus originating at the surface mixed layer are responsible for the maintenance of stratocumulus by supplying liquid water to the cloud layer [*Albrecht et al.*, 1995; *Bretherton and Pincus*, 1995]. Stratocumulus are known to cycle between horizontally inhomogeneous and homogeneous states, the former resembling trade wind cumulus fields [*Albrecht et al.*, 1995]. These transitions can be induced by cumulus forming below the cloud layer, cloud top entrainment, and drizzle [*Albrecht et al.*, 1995; *Feingold et al.*, 2010; *Korolev*, 1995; *Bretherton and Pincus*, 1995]. Cloud droplet formation in shallow cumulus is more strongly influenced by entrainment than in the core of stratocumulus decks [*Pruppacher and Klett*, 1997; R. Morales et al., Evaluation of a diabatic droplet activation parameterization using in-situ cloud data, submitted to *Journal of Geophysical Research*, 2010]. Thus, in real clouds, diabatic cloud droplet formation occurs much more frequently than adiabatic [e.g., *Chosson et al.*, 2007; *Gerber et al.*, 2005; *Grabowski and Pawlowska*, 1993; *Lin and Arakawa*, 1997; *Wang and Albrecht*, 1994; Morales et al., submitted manuscript, 2010], which is not recognized in most GCM studies of the indirect effect.

[7] Although there is a considerable body of work on entrainment effects on large-scale cumulus convection parameterization [e.g., *Morton et al.*, 1956; *Kain and Fritsch*, 1990; *Siebesma and Cuijpers*, 1995; *Randall et al.*, 2003; *Donner et al.*, 2001] less has been done on linking mixing processes with the microphysical parameters (primarily CDNC) of clouds in GCMs. Ideally, one would like to describe all of possible entrainment processes during the cloud lifetime (e.g., homogeneous [*Pruppacher and Klett*, 1997] and inhomogeneous mixing across all scales, and the droplet distribution changes that result [e.g., *Pruppacher and Klett*, 1997; *Brenguier and Chaumat*, 2001; *Morrison and Grabowski*, 2008]) (Figure 1a). This is very difficult, however, to determine, especially in a prescribed manner for inclusion in a subgrid parameterization. There may be a way, however, to describe the average cloud column properties that arise from the effects of cloud base activation and subsequent dilution and drying of droplets from entrainment. Toward this, *Barahona and Nenes* [2007] noted that mixing during the droplet activation process acts to decrease the cloud maximum supersaturation (hence activated CDNC) compared to adiabatic activation (Figure 1c). Adopting a homogeneous entrainment and mixing cloud model, *Barahona and Nenes* [2007] developed a droplet formation parameterization, using an "effective" per length entrainment rate, e that accounts for the effects of nucleation near cloud base and deactivation further up in the cloud column (Figure 1c). Using scaling arguments and microphysical observations of nonprecipitating cumulus, Morales et al. (submitted manuscript, 2010) concluded that the [*Barahona and Nenes*, 2007] formulation can describe cloud-average CDNC in entraining cumulus clouds when the average adiabaticity ratio (defined as the ratio of cloud liquid water content over the adiabatic value) is used to diagnose e. The same study also showed that for thick stratocumulus clouds, either adiabatic or diabatic formulations predict pdf-average CDNC to within experimental accuracy. Therefore, shallow and trade wind cumulus and stratocumulus are the main cloud types modified by this approach, the effects of which are most prominent in the tropics.

[8] In this work, we study the potential impact of entrainment on global CDNC, autoconversion rate, effective radius, and the first aerosol indirect effect [*Twomey*, 1977]. This is accomplished by implementing the *Barahona and Nenes* [2007] parameterization in the NASA Global Modeling Initiative (GMI) chemistry and transport model [*Meskhidze et al.*, 2007]. The sensitivity of global CDNC, cloud effective radius (R_{eff}), indirect forcing (IF) and auto-

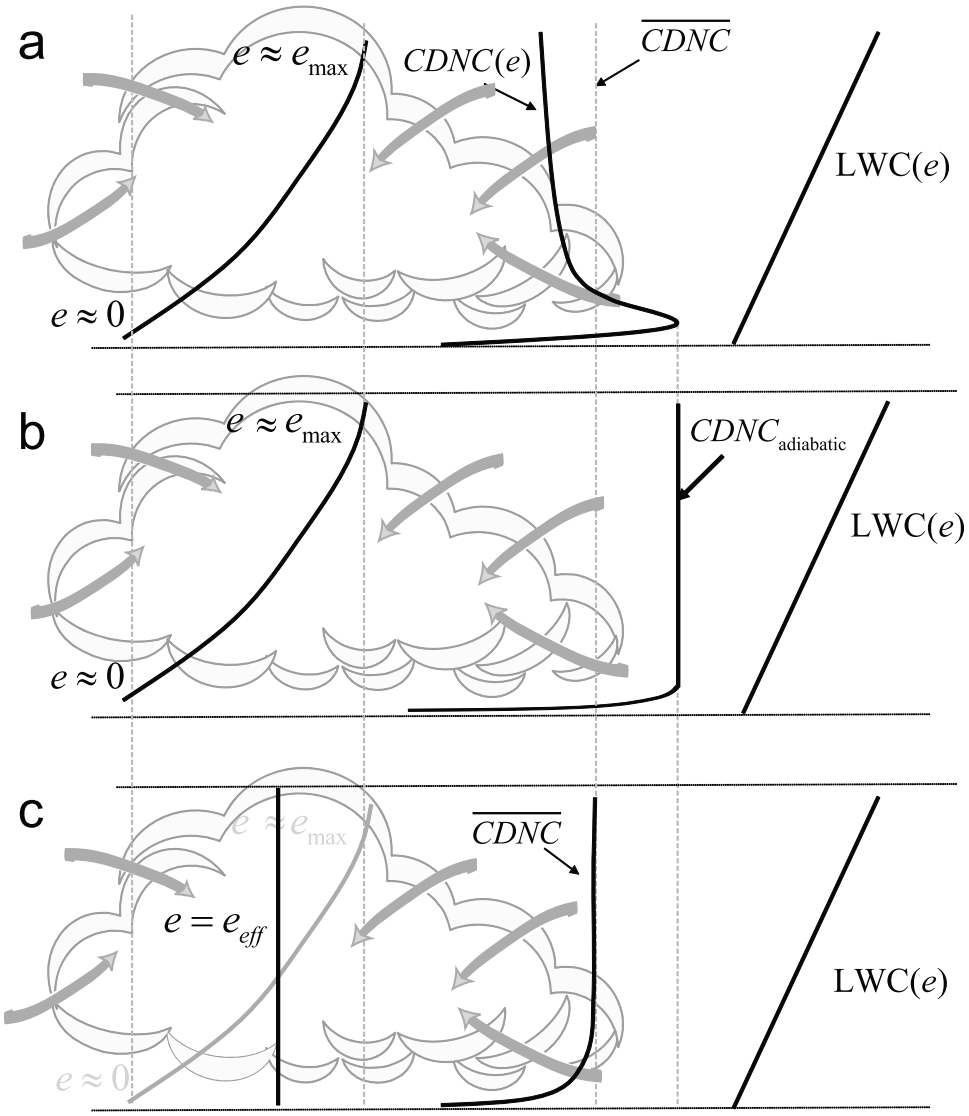

Figure 1. CDNC and LWC calculation in GCMs. (a) Representation of the entrainment profile in an ambient cloud where both LWC and cloud droplet activation are affected by entrainment. (b) Current GCM representation assuming adiabatic activation but LWC affected by entrainment. (c) The activation approach proposed in this study, where e is such so the cloud-average CDNC is similar to the ambient cloud in Figure 1a. Grey arrows represent entrainment of dry air.

conversion to diabatic activation is studied using different meteorological fields to drive the GMI model.

2. Model Description

[9] The NASA GMI model is a highly modular 3-D chemistry and transport model [*Rotman et al.*, 2001] capable of multiyear simulations for assessments of anthropogenic impacts on atmospheric chemistry. GMI computes the first-order response (i.e., without feedbacks of the cloud microphysics on the large-scale fields) of climate to external forcing and is therefore suitable for studying the first aerosol indirect effect [*Twomey*, 1977]. The modeling framework used is described by *Meskhidze et al.* [2007] and is summarized here. The aerosol module is coupled to the GMI-CTM advection core. Aerosol microphysics is not considered. Externally mixed prognostic aerosol species include sulfate, black carbon and organic matter from biomass burning and fossil fuel, organic matter from natural sources, mineral dust, and sea salt [*Liu et al.*, 2005, 2007]. The model considers primary emissions, chemical production of sulfate, gravitational sedimentation, dry deposition, wet scavenging, and hygroscopic growth [*Liu et al.*, 2005]. Anthropogenic and natural aerosol precursor emissions include SO_2, organic matter, black carbon, oceanic DMS, dust and sea salt [*Liu et al.*, 2005; *Meskhidze et al.*, 2007].

[10] Two types of clouds exist in GMI: convective and large-scale (stratocumulus and trade wind cumulus); clouds are allowed to form in any model layer with the exception of the layer nearest to the surface, as it is very shallow (formation

of fog is not considered). Large-scale cloud fraction is diagnosed based on the grid cell relative humidity [*Hack*, 1998], RH, using a threshold relative humidity for condensation specified as a function of pressure [*Xu and Krueger*, 1991]. For convective cloud fraction, a parameterization with convective mass flux [*Xu and Krueger*, 1991] was adopted. Total cloud fraction in each layer is obtained from the combination of the large-scale cloud fraction and convective cloud fraction assuming random mixing [*Feng et al.*, 2004], which has been shown to adequately reproduce the observed global distribution of liquid water path. Following *Hack* [1998], the cloud liquid water content (LWC) is vertically distributed using a cloud liquid water density profile [*Kiehl*, 1994] derived from experimental measurements and GCM simulations. In-cloud liquid water path (LWP) at each level is found by the integration of LWC between layers [*Meskhidze et al.*, 2007]. Cloud forcing and radiative properties are calculated online using the CLIRAD-SW solar radiative transfer model [*Chou et al.*, 1998], which gives the cloud optical depth and the shortwave radiative flux from the surface to the top of the atmosphere (TOA). Radiative fluxes are integrated over the solar spectrum, from 0.175 μm to 10 μm. Inputs in the radiative transfer module include the cloud droplet effective radius, the in-cloud LWC, the cloud fraction, the specific humidity and the O_3 concentrations for each grid box as well as the surface albedo for the direct and diffuse light and the solar zenith angle. Aerosol indirect forcing (IF) is calculated as the difference in the TOA net outgoing shortwave radiative flux between two simulations, usually between those with "present-day" (natural and anthropogenic) and "preindustrial" (only natural) emissions of aerosols (and their precursors). In computing indirect forcing, surface albedo for direct and diffuse light was obtained from the GEOS4 GCM [*Bloom et al.*, 2005]. Following *Del Genio et al.* [1996], liquid clouds were those with a cloud top temperature above 263.15 K over land, and, 269.15 K over ocean. The sensitivity of indirect forcing to the meteorological field (used to diagnose grid cell RH, T and p) is assessed by carrying out simulations with fields from the former NASA Data Assimilation Office (DAO), the NASA finite volume GCM (FVGCM), and the Goddard Institute for Space Studies version II' (GISS) GCM. Each of the archived meteorological data sets spans over 1 year.

[11] The horizontal resolution in all simulations is, 4° latitude by 5° longitude. Vertical resolution differs in each meteorological field, being 46, 42, and 23 layers for DAO, FVGCM, and GISS, respectively. Monthly and annually averaged CDNC, R_{eff}, and autoconversion rates (Q_{aut}) are computed from the simulations. Simulations with GMI are carried out for each meteorological field (DAO, GISS, FVGCM) using both "present day" (i.e., all emissions active) and "preindustrial" (i.e., emissions active except anthropogenic) emissions.

2.1. Description of Cloud Parameterizations

[12] CDNC is assumed equal to the nucleated droplet number which is supported by field campaign studies [e.g., *Conant et al.*, 2004; *Guibert et al.*, 2003; *Lu et al.*, 2008; *Meskhidze et al.*, 2005; *Peng et al.*, 2005] and justified as precipitating cumulus and stratocumulus clouds typically have short lifetimes [*Pruppacher and Klett*, 1997]. Cloud droplet number is calculated using the parameterization of *Barahona and Nenes* [2007, hereafter BN07], which explicitly includes the effects of entrainment and mixing on maximum supersaturation and CDNC. BN07 is an extension of the works of *Nenes and Seinfeld* [2003] and *Fountoukis and Nenes* [2005]; it can treat the effects of externally mixed aerosol, CCN containing surfactants and slowly growing droplets (expressed by changes in the water vapor mass transfer coefficient). This parameterization has been shown to reproduce in situ measurements of CDNC in cumulus and stratocumulus clouds [*Meskhidze et al.*, 2005; *Fountoukis et al.*, 2007; Morales et al., submitted manuscript, 2010]. In this study, the effect of aerosol equilibrium liquid water content on supersaturation is neglected (i.e., the "simplified" version of BN07 is used). This assumption introduces less than 1% error in CDNC calculation for pristine and moderately polluted environments (aerosol mass less than 102 μg m^{-3}) and cloud-free air conditions far from saturation (RH < 95%), which characterizes most of the atmosphere. With these assumptions, BN07 involves finding the root of the local supersaturation tendency equation [*Barahona and Nenes*, 2007],

$$\frac{ds}{dt} = \alpha V\left(1 - \frac{e}{e_c}\right) - \gamma\left(\frac{dW}{dt}\right) = 0 \tag{1}$$

where V is the updraft velocity, s is the supersaturation, $\frac{dW}{dt}$ is the rate of condensation of liquid water onto the drops, determined using the method of "population splitting" as described by *Nenes and Seinfeld* [2003], *Fountoukis and Nenes* [2005], and *Barahona and Nenes* [2007]. The critical entrainment rate, e_c, is defined as the entrainment rate that completely prevents droplet activation (i.e., the upper limit in e for which cloud formation is possible) given by [*Barahona and Nenes*, 2007],

$$e_c = \frac{\alpha}{(1 - RH) - \frac{\Delta H_v M_w \Delta T}{RT^2}} \tag{2}$$

where $\alpha = \frac{gMw\Delta H_v}{c_p RT^2} - \frac{gM_a}{RT}$, RH is the ambient relative humidity and ΔT is the difference between cloud and ambient temperatures. Parcel model simulations show that entrainment would affect CCN activation if $e/e_c > 0.1$ [*Barahona and Nenes*, 2007]; adiabatic activation occurs when $e = 0$ (i.e., negligible mixing rate). The value of s determined from equation (1) corresponds to the maximum supersaturation, $s_{\max}$. The droplet number concentration is then calculated as the CCN with critical supersaturation less than $s_{\max}$. BN07 evaluated the parameterization against a detailed numerical parcel model over a wide set of cloud forming conditions that included entrainment; the mean relative error in computed CDNC was 2 ± 21%.

[13] In principle, equation (1) is also applicable to homogeneous mixing in convective clouds, and may provide a simple way to parameterize entrainment in large-scale convection schemes. Equation (1) is derived assuming that mixing between cloudy and cloud-free air is instantaneous and homogeneous. In our approach, e and e/e_c therefore represent "effective" mixing rates (Figure 1) that would account for the net effect of mixing processes throughout the cloud column, i.e., the reduction in CDNC with respect to

Table 1. Dry Aerosol Size Distributions Used in This Study [*Lance et al.*, 2004][a]

Aerosol Mode	Marine			Continental		
	Nuclei	Accumulation	Coarse	Nuclei	Accumulation	Coarse
$\frac{N_i}{N_{tot}}$	0.561	0.432	0.008	0.555	0.444	4×10^{-4}
D_{gi}	0.02	0.092	0.58	0.01	0.067	0.93
σ_{gi}	1.47	1.6	2.49	1.6	2.1	2.2
ϵ_{sol}	0.33	0.33	0.95	0.5	0.5	0.5

[a] D_{gi}, σ_{gi}, and ϵ_{sol} is the geometric mean diameter (μm), spectral width, and soluble fraction, respectively. N_i is the number concentration of mode "i", and N_{tot} is total number concentration in the population.

adiabatic activation. This is justified as the GMI model simulates cloud-scale averages over relatively large grid cells and time steps. From the CDNC perspective, this approach captures cloud-column average CDNC better than the adiabatic value in trade wind cumulus and stratocumulus (Morales et al., submitted manuscript, 2010). The extension of this approach when inhomogeneous mixing and partial droplet evaporation significantly impact CDNC requires an analysis using ambient cloud data and will be the subject of a future study.

[14] Autoconversion rate of cloud water to rain is computed from the scheme of *Khairoutdinov and Kogan* [2000], which is derived from large eddy simulations of drizzling stratocumulus clouds. Autoconversion rate (s^{-1}) is given by

$$Q_{aut} = 1350\left(\frac{q_l}{C_l}\right)^{2.47}(CDNC)^{-1.79} \quad (3)$$

where C_l is the cloud fraction and q_l the liquid water mass mixing ratio; CDNC is in cm^{-3}. *Hsieh et al.* [2009a] showed that among several parameterizations commonly used in GCM studies, equation (3) has the strongest dependency on CDNC, hence it can express the upper limit of autoconversion sensitivity to CDNC from entrainment. Q_{aut} is used as a diagnostic of the potential effect of diabatic activation on the cloud lifetime and precipitation rate. However, as no feedback is considered between CDNC and LWC, Q_{aut} is only meaningful for the comparison between diabatic and adiabatic cases.

2.2. Implementation of the Cloud Activation Parameterization

[15] Calculation of CDNC using BN07 requires the knowledge of T, p, aerosol size distribution and composition, V, e, ΔT and cloud-free air RH. The characteristic cloud formation T and p [*Barahona and Nenes*, 2007] are taken as the grid-cell average T and p. Grid-cell average RH is assumed to be representative of the cloud-free air entrained in the cloudy columns. ΔT is estimated from the release of latent heat during condensation [*Paluch*, 1979; *Seinfeld and Pandis*, 1998]; an energy balance applied to a cloudy parcel at steady state then gives,

$$\Delta T \approx \left(\frac{\Delta H_v}{c_p}\right)\left(\frac{q_l}{C_l}\right) \quad (4)$$

Application of equation (4) provides a global average $\Delta T \simeq$ 0.4 K for the three meteorological fields (DAO, GISS, and FVGCM), with ΔT in marine environments being slightly higher (~0.5 K) due to the larger LWC in these regions (not shown).

[16] Calculation of CDNC requires knowledge of the aerosol size distribution and hygroscopicity. As currently GMI simulates only aerosol mass, distributions are diagnosed from the online simulation by scaling distributions obtained from observations [*Lance et al.*, 2004] using the predicted sulfate mass. In these distributions, aerosol over marine regions is composed of 67% insoluble material and 33% ammonium sulfate in the fine mode, and, 95% sea salt and 5% insoluble material in the coarse mode. Aerosol over land is composed of 50% insoluble material and 50% ammonium sulfate in both the coarse and fine modes [*Lance et al.*, 2004]. The size distribution mode diameter, geometric standard deviation, and number concentration for marine and continental aerosol are given in Table 1. Chemical effects on hygroscopicity are also important [*Lance et al.*, 2004; *Nenes et al.*, 2002; *McFiggans et al.*, 2005]; however, they are not considered in this study to facilitate the interpretation of the effects of entrainment on droplet activation. The effect of assuming a constant aerosol size distribution is discussed in section 4.

[17] This study adopts two approaches to diagnose e. In the first one, adiabaticity (i.e., the ratio of in-cloud LWC to its adiabatic value; [*Kim et al.*, 2008]) is assumed constant and used as proxy for e/e_c. Morales et al. (submitted manuscript, 2010) have shown that this approach can give good CDNC closure if $1 - e/e_c$ is set equal to the cloud-average adiabaticity. Recent in situ observations report ~0.5–0.6 adiabaticity for small cumulus clouds [*Lu et al.*, 2008; Morales et al., submitted manuscript, 2010]; thus entrainment effects on CDNC, IF, and Q_{aut} are studied by carrying out simulations with effective e equal to $0.0e_c$ (adiabatic), $0.4e_c$, and $0.6e_c$. We also directly specify e, using average values derived from LES simulations of shallow convective clouds [*Siebesma and Cuijpers*, 1995]; $e = 2 \times 10^{-3}$ m^{-1} for positively buoyant cloudy parcels ("core" case), and, $e = 3 \times 10^{-3}$ m^{-1} for all cloud parcels with positive LWC and V ("updraft" case). Similar e values have been reported in other published studies that reflect changes in a variety of dynamical conditions [e.g., *McCarthy*, 1974; *Raga et al.*, 1990; *Gregory*, 2001; *Neggers et al.*, 2003], so $e = 2 \times 10^{-3} - 3 \times 10^{-3}$ m^{-1} can be considered representative of the global average. Using a fixed, average e/e_c implies a spatial variation in e (as e_c depends on local RH and T, equation (2)) whereas maintaining e constant implies a spatial variation in e/e_c; thus, the two approaches used represent limits of variability in both e and e/e_c.

[18] In addition to the aerosol size distribution and e, CDNC calculation requires the knowledge of cloud-scale V. Since this is not directly available in large-scale models, we prescribe V using values from field campaign studies; an average V is thus prescribed for "continental" and "marine"

Table 2. Global Mean CDNC, R_{eff}, Q_{aut}, and IF for Runs Using Adiabatic Activation[a]

	DAO	GISS	FVGCM	σ
CDNC (cm^{-3})	102.6	96.3	95.6	21.4
R_{eff} (μm)	8.2	8.9	7.5	0.37
$\log(Q_{aut})$	−10.3	−10.2	−10.4	0.32
IF (W m^{-2})	−1.28	−1.30	−1.75	0.33

[a]The standard error, σ, was calculated as the global mean standard deviation from the average of the three meteorological fields.

clouds equal to 1 m s^{-1} and 0.35 m s^{-1}, respectively [*Lance et al.*, 2004; *Peng et al.*, 2005; *Fountoukis et al.*, 2007] for droplet activation in stratocumulus. A single V can express the vertical velocity distribution average droplet number in cumulus and stratocumulus clouds, provided that it expresses the average updraft velocity distribution in the boundary layer [*Lance et al.*, 2004; *Meskhidze et al.*, 2005; *Peng et al.*, 2005; *Fountoukis et al.*, 2007; *Morales and Nenes*, 2010]. Although this approach can provide realistic droplet distributions [*Chen et al.*, 2010]; vertical velocity is nevertheless treated as an adjustable parameter.

3. Results

[19] Entrainment reduces $s_{\max}$ hence the number of activated CCN (CDNC). The extent of the CDNC reduction (compared to assuming adiabatic activation) depends primarily on e/e_c and the characteristics of the aerosol population [*Barahona and Nenes*, 2007]. Simulations are carried out varying e (using both methods outlines in section 2.2) in the CDNC parameterization but maintaining the (diabatic) LWC as given by GMI (section 2). This allows quantifying the error associated with neglecting entrainment effects on CDNC, R_{eff}, IF and Q_{aut}.

[20] Entrainment effects are expressed in terms of an absolute change,

$$\Delta X_{abs} = X - X_{ad} \tag{5}$$

where X refers to the annual average of the variable being analyzed (e.g., CDNC, IF) calculated for diabatic activation, and X_{ad} refers to its value assuming adiabatic activation (i.e., $e = 0$). Entrainment effects on X are also expressed in relative terms as

$$\Delta X_{rel} = \frac{\Delta X_{abs}}{X_{ad}}\% \tag{6}$$

3.1. CDNC, Q_{aut}, and IF Under Adiabatic Activation

[21] The global distribution of CDNC, IF, and Q_{aut} calculated assuming adiabatic activation (i.e., $e = 0$) are presented in Figure 2 and summarized in Table 2. For the meteorological fields used in this study, high CDNC is found near heavily polluted areas of the Northern Hemisphere (NH) (i.e., China, western Europe, eastern coast of the U.S. and the Gulf of Mexico), consistent with the high level of aerosol associated with industrialized regions, and, is the lowest over the polar regions. The influence of long-range transport of aerosol is reflected in the higher CDNC in the Northern Hemisphere than in the Southern Hemisphere. In the latter, high CDNC is associated with biomass burning emissions over the continents, and, enhanced sulfate production from DMS oxidation over the oceans.

[22] Usage of DAO results in the highest global average CDNC (~102 cm^{-3}), whereas the lowest is found with FVGCM (~95 cm^{-3}). Table 2 presents the standard error for the comparison, calculated as the mean annual average of the standard deviation between the three meteorological fields. The large variation in CDNC between the three meteorologies (~21 cm^{-3}) indicate that the difference between global means may not be statistically significant; local differences, however, may be much higher. Among the meteorological fields used, DAO has the strongest low-level poleward transport toward the NH and the weakest wet scavenging, resulting in larger aerosol load in the NH than with the other fields [*Liu et al.*, 2007]. Similarly, runs with FVGCM exhibit the largest CDNC in the Southern Hemisphere due to larger DMS emissions and stronger poleward transport in FVCGM than in the other fields [*Liu et al.*, 2007].

[23] The variability in CDNC and LWC among meteorological fields results in ~1 ± 0.37 μm variation in R_{eff}. The spread about the mean is, however, much lower than for CDNC (Table 2) and the differences are significant to a 90% level (given by a student t test). R_{eff} is typically 1–2 μm larger over the ocean than over the continents, which reflects the larger LWC (and smaller CDNC) in marine than in continental regions [*Seinfeld and Pandis*, 1998]. These values are, however, about 1–2 μm smaller than typically observed in satellite retrievals [*Bennartz*, 2007; *Chang and Li*, 2002] (e.g., Figure 9, section 3.5) although in better agreement with ground-based measurements [*Dong et al.*, 1997], suggesting that while adiabatic activation is reflective of cloud-base CDNC, it may lead to overestimation of column-average and cloud-top CDNC (hence underestimating satellite-retrieved R_{eff}) [*Chang and Li*, 2002]. Local variation in CDNC and LWC results in over 4 orders of magnitude variation in Q_{aut} (Figure 2), being about 10^{-9} s^{-1} over the southern oceans and as low as 10^{-12} s^{-1} in North Africa and East Asia, and higher in the SH than in the NH. There is little variation in global mean Q_{aut} among meteorological fields; local differences though can be high, particularly in the tropics, where DAO and GISS result in a factor of 10 higher Q_{aut} than for FVGCM.

[24] The global mean IF ranges between −1.28 W m^{-2} (DAO) and −1.75 W m^{-2} (FVGCM). As no feedbacks between CDNC and LWC are considered in the GMI model, the magnitude of the IF predicted is slightly higher than current estimates of about −0.7 ± 0.5 W m^{-2} [*Quaas et al.*, 2009]. Thus, IF in Figure 2 represents the first-order response (i.e., without feedbacks of CDNC on LWC) of shortwave radiative flux to anthropogenic aerosol emissions. The largest values of IF are found over SE Asia, western Europe and eastern United States consistent with areas of high anthropogenic sulfur emissions. High IF (although smaller than in the NH) are also found in industrialized centers as well as in biomass burning regions of the SH. All meteorological fields result in larger IF over the continents than over the oceans; long-range transport of pollution plumes, however, leads to appreciable IF far into oceanic regions, particularly for the DAO and FVGCM fields. The

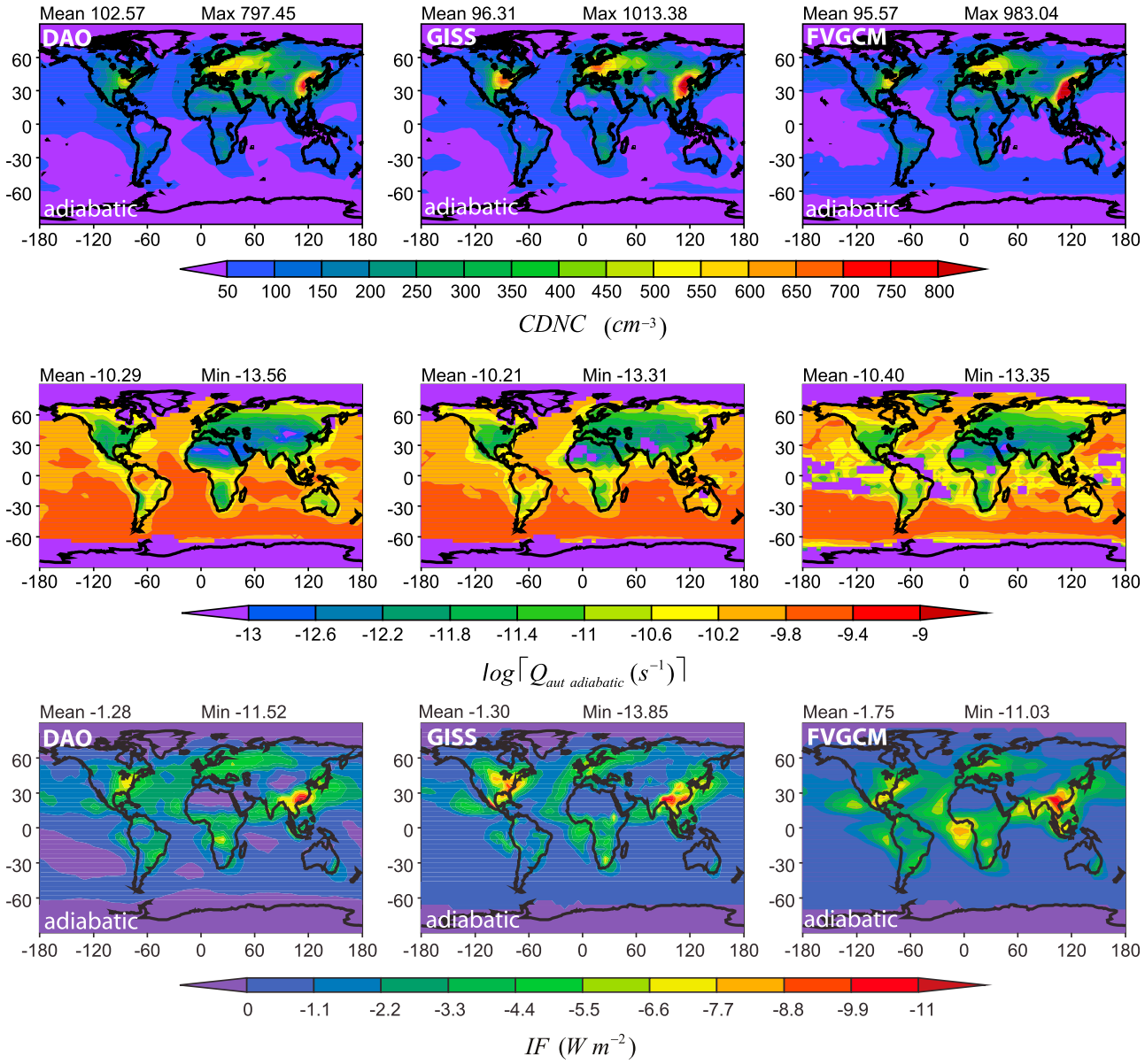

Figure 2. Cloud droplet number concentration (CDNC), autoconversion rate Q_{aut}, and indirect forcing (IF) under adiabatic activation (i.e., $e = 0$).

runs presented in Figure 2 represent the control case used to study entrainment effects on droplet activation.

3.2. CDNC Under Diabatic Activation

[25] Considering entrainment leads to lower CDNC than in simulations assuming adiabatic droplet activation (Figure 3 and Table 3). The global annual mean ΔCDNC_{rel} lies between −10% and −12% for $e = 0.4e_c$, and, from −17% to −21% for $e = 0.6e_c$. ΔCDNC_{abs} (equation (4)) ranges between −13 and −15 cm^{-3} for $e = 0.4e_c$, and, from −23 to −25 cm^{-3} for $e = 0.6e_c$; for the latter the minimum ΔCDNC_{abs} is close to −350 cm^{-3} (not shown).

[26] Consistent with parcel model simulations, areas with high CCN concentrations (i.e., high adiabatic CDNC, Figure 2), associated with regions of aerosol sources, tend to display large absolute changes in CDNC from entrainment effects (where ΔCDNC_{abs} is generally around −200 cm^{-3}; Figure 3). The largest ΔCDNC_{rel} (which is most relevant for changes in SW cloud forcing) is, however, found in the tropics, downwind of large emission sources, and in South America and North Africa (Figure 3). Thus, clouds with moderate CDNC (100–300 cm^{-3}) are relatively more sensitive to entrainment than clouds formed in very polluted regions.

[27] The high sensitivity of CDNC to entrainment in moderately polluted regions is explained by the sensitivity of CDNC to $s_{\max}$, which is equal to the slope of the CCN spectrum (i.e., the function relating the number of CCN with s) at $s_{\max}$. CCN spectra for single modal aerosol tend to have a sigmoidal shape [e.g., *Twomey*, 1977;

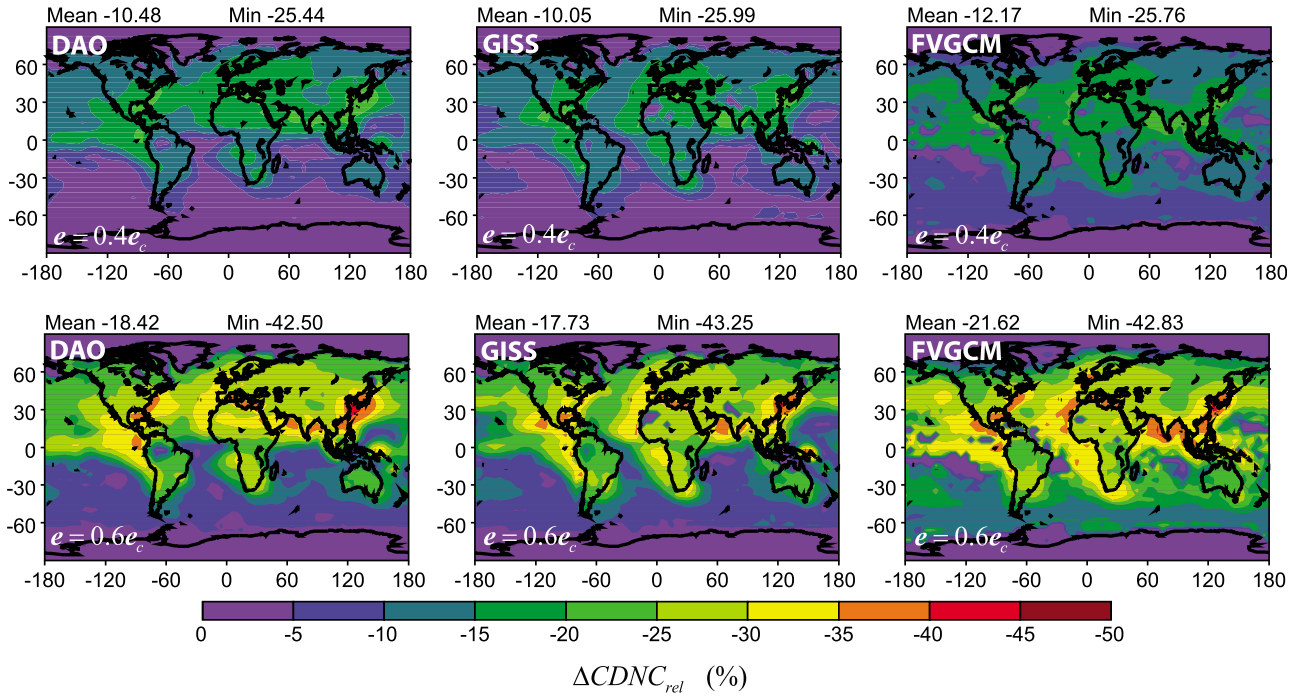

Figure 3. Annual mean ΔCDNC_{rel} for (top) $e = 0.4e_c$ and (bottom) $e = 0.6e_c$. Simulations were carried out using (left) DAO, (middle) GISS, and (right) FVGCM meteorology.

Medina et al., 2007], the supersaturation range where roughly half of the particles act as CCN exhibits the highest sensitivity to s (i.e., $\frac{dCCN}{ds}$, hence $\frac{dCDNC}{ds}$ is high). For multimodal aerosol the region of maximum sensitivity to s is usually located at lower activation fraction, as the coarse and accumulation modes tend to activate at lower s than the nucleation mode (Figure 4). For high supersaturations, a significant fraction of particles activate so $\frac{dCCN}{ds} \rightarrow 0$. At low supersaturations, the activation fraction and $\frac{dCCN}{ds}$ are small. Thus, if high $s_{\max}$ is reached CDNC is not very sensitive to small variations in $s_{\max}$. Figure 4 shows that for the continental and marine aerosol distributions of Table 1 the region of maximum $\frac{dCCN}{ds}$ corresponds to an activated fraction around 0.1. A second mode of $\frac{dCCN}{ds}$ is also evident around s = 2% ($\frac{CCN}{CN}$ about 0.6) which is more prominent for the marine aerosol.

[28] Since high $s_{\max}$ (hence high activation fraction) is characteristic of very clean marine environments, ΔCDNC_{rel} and ΔCDNC_{abs} are low there (Figure 5). For higher aerosol loads (i.e., near the tropics), CDNC is sensitive to variations in $s_{\max}$, as the CCN spectrum is steep (fraction of particles acting as CCN between 0.2 and 0.5). However, for polluted regions (e.g., regions of high sulfur emission in the NH), $s_{\max}$ is low and the CCN spectrum is somewhat insensitive to changes in $s_{\max}$ (fraction of particles acting as CCN below 0.1, Figure 5). ΔCDNC_{rel} remains relatively high at lower activation fraction than ΔCDNC_{abs} as low adiabatic CDNC tends to increase the sensitivity of ΔCDNC_{rel} to CDNC (equation (4)).

[29] Among the meteorological fields used, ΔCDNC_{rel} is the largest for FVGCM and the lowest for GISS (Figure 3 and Table 3), reflecting differences in aerosol concentration between meteorological fields [*Liu et al.*, 2007]. Simulations using DAO and FVGCM result in moderate CDNC concentrations (100–300 cm^{-3}), hence significant ΔCDNC_{rel} over large regions of the NH. A similar spatial variation is found using GISS (Figure 3), although ΔCDNC_{rel} is relatively lower. Compared to simulations with DAO and GISS, the usage of FVGCM fields results in higher values of ΔCDNC_{rel} over the southern Atlantic Ocean. Figure 5 shows significant scatter of ΔCDNC_{abs} and ΔCDNC_{rel} for all meteorological fields, reflecting

Table 3. Global Mean (Maximum) Deviation From Results of Adiabatic Simulation

Field	$e = 0.4e_c$			$e = 0.6e_c$			$e = 2 \times 10^{-3}$ m^{-1}	$e = 3 \times 10^{-3}$ m^{-1}
	DAO	GISS	FVGCM	DAO	GISS	FVGCM	GISS	GISS
ΔCDNC_{abs} (cm^{-3})	−14.7(−151.1)	−13.4(−196.8)	−14.7(−189.8)	−25.8(−261.2)	−23.5(−345.0)	−25.8(−333.2)	−19.5(−210.2)	−32.6(−363.1)
ΔCDNC_{rel} (%)	−10.4(−25.4)	−10.0(−26.0)	−12.1(−25.8)	−18.4(−42.5)	−17.7(−43.2)	−21.6(−42.8)	−13.5(−55.8)	−21.0(−87.0)
$\Delta R_{eff,abs}$ (μm)	0.25(0.59)	0.22(0.58)	0.21(0.58)	0.48(1.19)	0.43(1.15)	0.41(1.16)	0.33(2.05)	0.62(3.72)
$Q_{aut}/Q_{aut,ad}$	1.12(1.63)	1.09(1.54)	1.11(1.58)	1.26(2.53)	1.20(2.30)	1.25(2.40)	1.18(3.94)	1.70(32.5)
ΔIF_{abs} (W m^{-2})	0.19(1.18)	0.16(1.22)	0.17(1.17)	0.39(2.21)	0.32(2.47)	0.35(2.34)	0.23(2.13)	0.40(3.45)
ΔIF_{rel} (%)	−19.6(−90.1)	−21.6(−80.1)	−15.0(−92.5)	−31.4(−99.2)	−40.4(−98.8)	−29.4(−98.4)	−25.1(−80.5)	−43.1(−99.5)

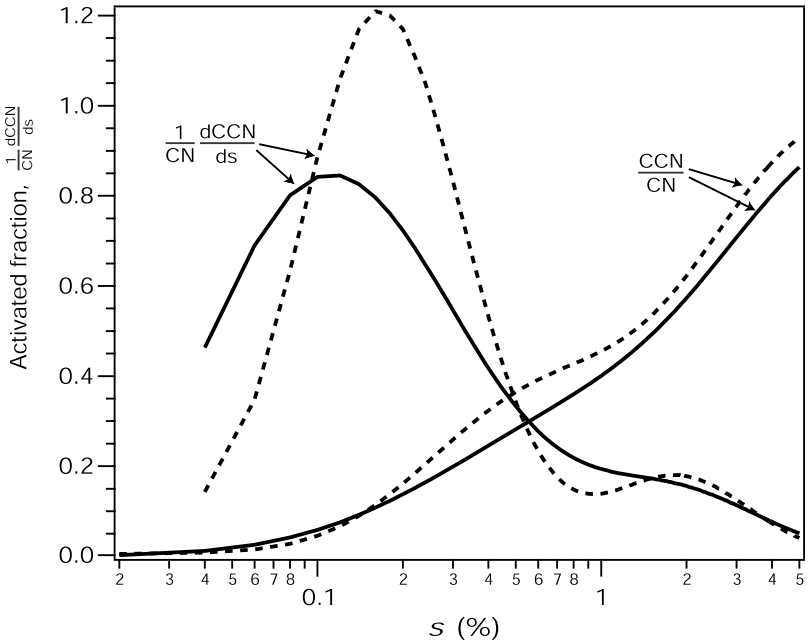

Figure 4. CCN activation spectra for the continental (solid line) and marine (dashed line) aerosol distributions of Table 1.

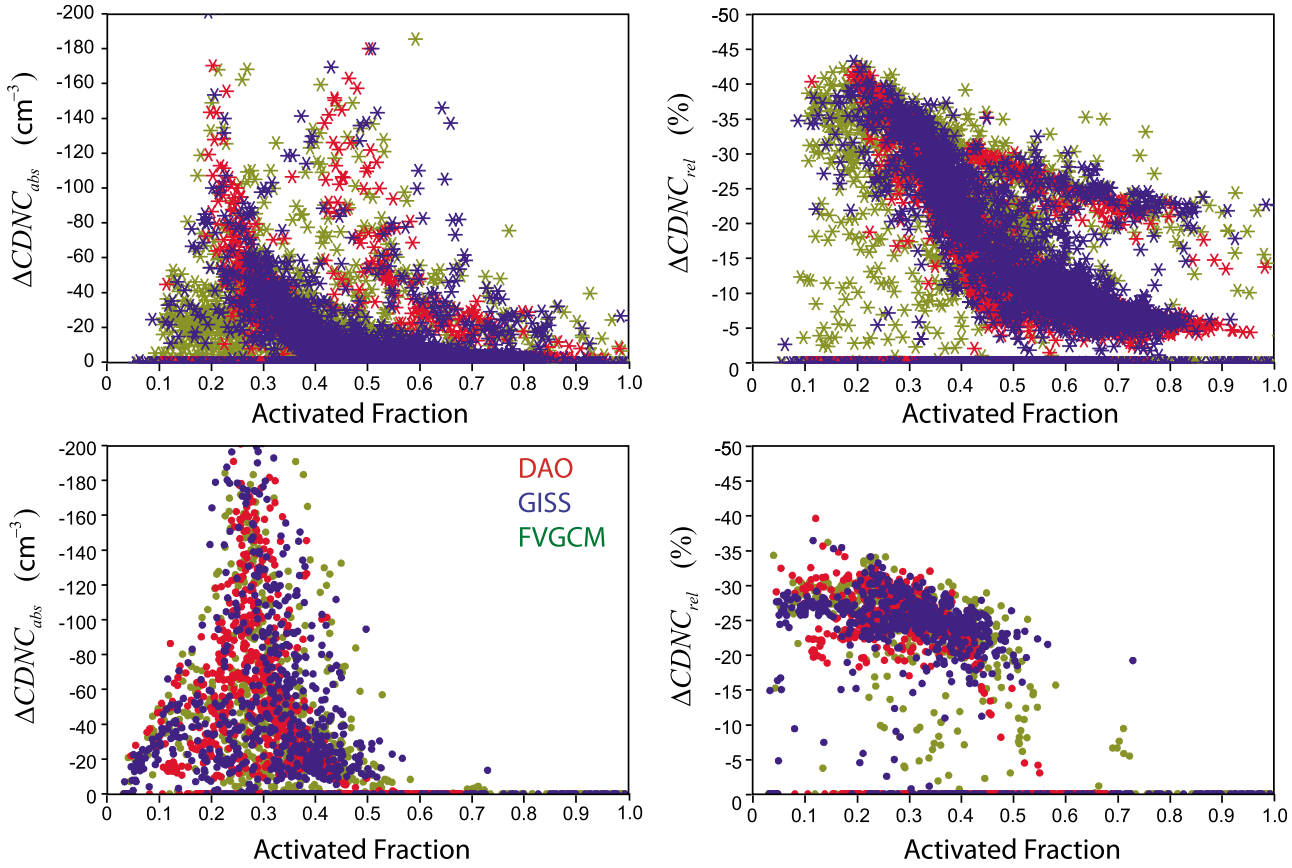

Figure 5. (left) $\Delta\mathrm{CDNC}_{abs}$ and (right) $\Delta\mathrm{CDNC}_{rel}$ against activated fraction for $e = 0.6e_c$. Results are presented for (top) ocean and (bottom) land.

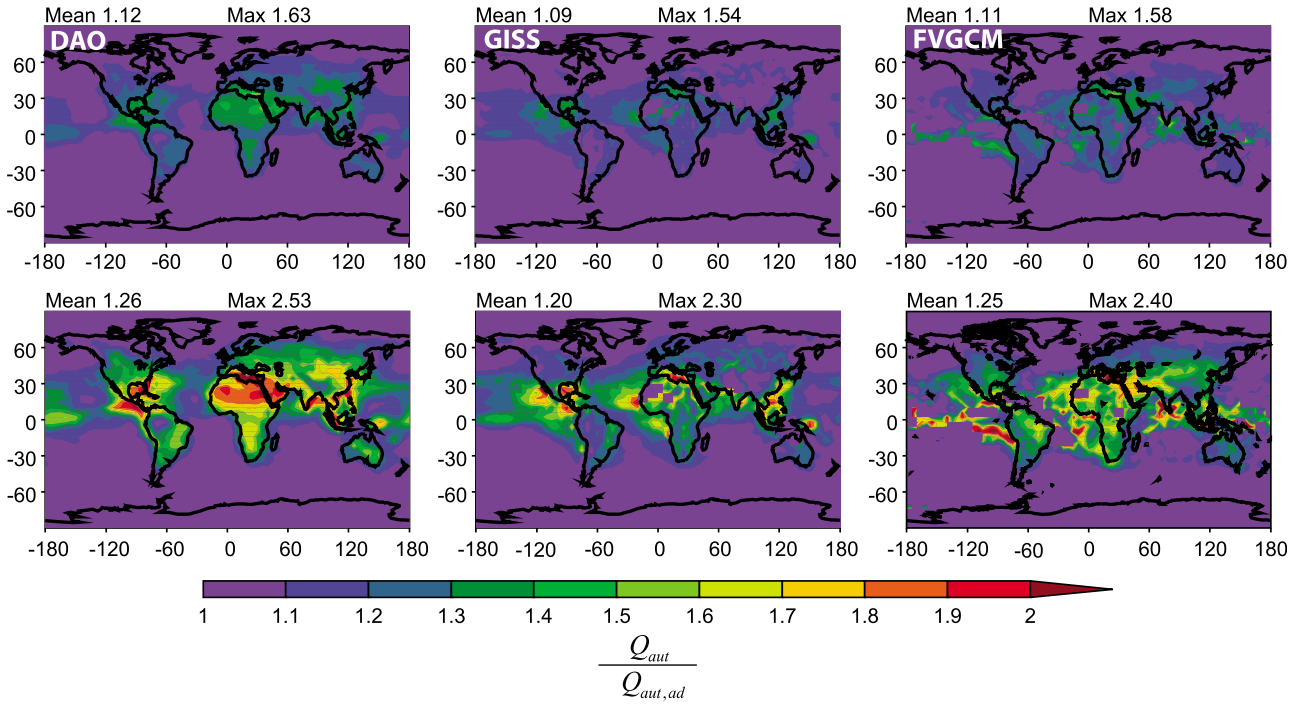

Figure 6. Similar to Figure 3, but for $\frac{Q_{aut}}{Q_{aut,ad}}$.

the large variability of aerosol concentration in marine and continental environments, and the influence of local *RH* and *T*.

3.3. Effective Radius and Autoconversion Rate

[30] Compared to adiabatic activation, entrainment reduces CDNC and yields a larger effective radius. Thus, $\Delta R_{eff,abs}$ reflects the bias that is introduced when adiabatic activation is assumed to represent cloud-column CDNC. Table 3 shows the mean and maximum global R_{eff} for the meteorological fields and range of e considered in this study. Large areas over the tropics (associated with high LWC and moderate CDNC) are characterized by $\Delta R_{eff,abs} \sim 1$ μm (e.g., Figure 9). For all meteorological fields used in this study global mean $\Delta R_{eff,abs}$ ranges between 0.21 and 0.48 μm for $e = 0.4e_c$ and $e = 0.6e_c$, respectively.

[31] According to equation (3), lower CDNC implies higher Q_{aut} if q_l and C_l are constant. This is shown in Figure 6, which presents the ratio of Q_{aut} to its "adiabatic" value $Q_{aut,ad}$ (i.e., for $e = 0$). Neglecting entrainment effects on droplet activation would decrease global Q_{aut} around 10% for $e = 0.4e_c$ and around 23% for $e = 0.6e_c$ (Table 3); locally, Q_{aut} can be affected by up to a factor of two. Thus, including entrainment effects on CDNC increases the autoconversion rate, thus reducing the amount of tuning required for a realistic climate simulation [*Chen et al.*, 2010]. However, if the increased entrainment is accompanied with an increased rate of droplet evaporation, the net increase in Q_{aut} may be negligible [e.g., *Jiang et al.*, 2006; *Wood*, 2007]. Although the global mean $Q_{aut}/Q_{aut,ad}$ is similar for all meteorological fields used, the regional $Q_{aut}/Q_{aut,ad}$ is the largest in Central America and northern Africa for the DAO simulation whereas for GISS and FVGCM it is the largest in the tropical Atlantic and Pacific oceans. This is explained by the slightly larger ΔCDNC_{rel} in marine environments for simulations with the FVGCM and GISS fields, compared to the DAO simulations (Figure 3).

3.4. Indirect Forcing

[32] The variation of CNDC and R_{eff} with e suggests that cloud radiative properties would respond nonlinearly to entrainment, therefore affecting IF [*Kim et al.*, 2008]. The low slope of the CCN spectrum at high $s_{\max}$ (Figure 4) implies that CDNC is less sensitive to entrainment during preindustrial conditions (because low aerosol loads mean a higher activation ratio than for present day). Simulations support this; ΔCDNC_{rel} in the preindustrial simulation is lower than for present-day simulations, reaching global means around −4% and −8% for $e = 0.4e_c$ and $e = 0.6e_c$, respectively. Thus, the magnitude of IF computed for diabatic activation would be lower than when adiabaticity is assumed.

[33] Figure 7 presents the annual average ΔIF_{abs} for all meteorological fields of this study. Global mean ΔIF_{abs} ranges from ~0.17 W m^{-2} to ~0.39 W m^{-2} (Table 3). ΔIF_{rel} may reach values around −80% in areas of the tropics with very low adiabatic IF. In terms of the absolute reduction in IF, ΔIF_{abs} is the strongest (~2.4 W m^{-2}) in regions with moderate adiabatic IF (~5 W m^{-2}). In pristine regions, ΔIF_{rel} tends to be very sensitive to changes in IF as adiabatic IF is very low (equation (4) and Figure 2). These zones coincide with low adiabatic CDNC, and ΔIF_{rel} is the largest at very low CDNC, consistent with the high susceptibility of cloud albedo to CDNC in clean clouds [*Twomey*, 1991]. However, ΔIF_{rel} decreases below −10% for CDNC greater than 300 cm^{-3} (not shown). The largest ΔIF_{abs} is found at moderate CCN concentrations where ΔCDNC_{rel} is largest (~−40%). Because of this, marine environments with mod-

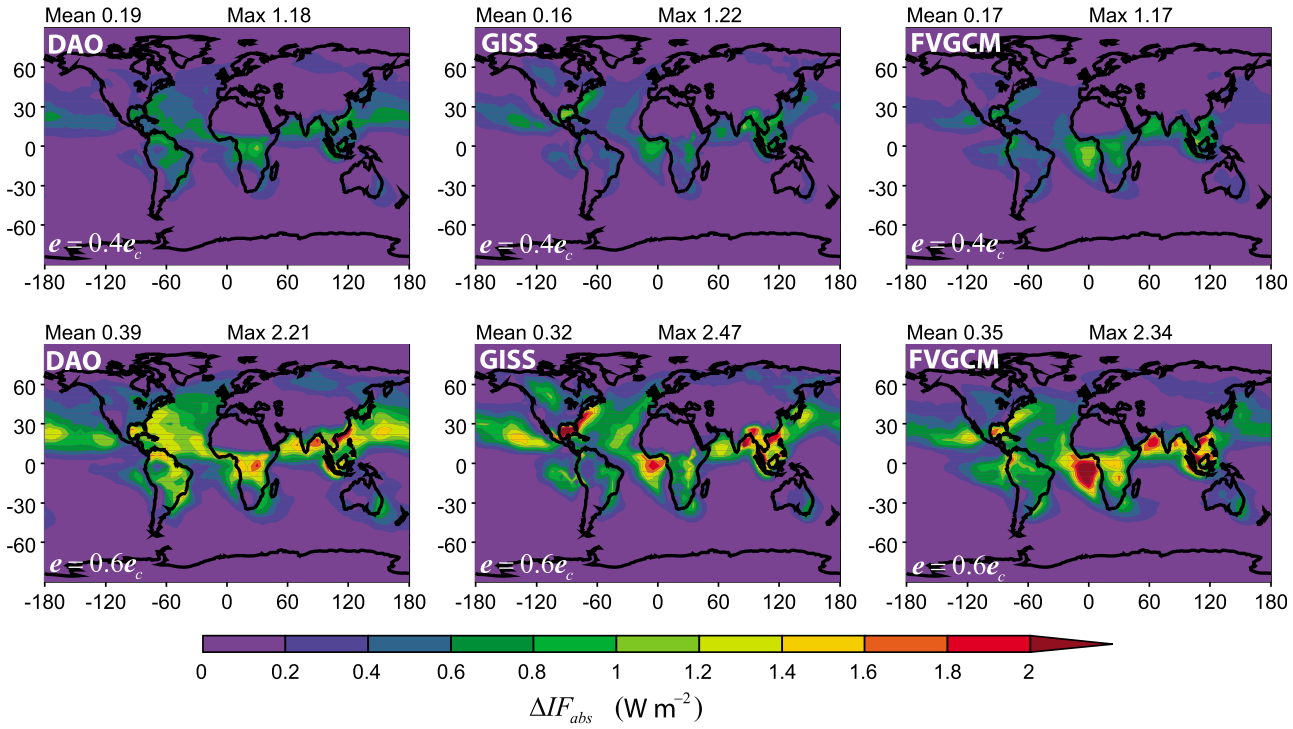

Figure 7. Similar to Figure 3, but for ΔIF_{abs}.

erate CCN concentration display a larger ΔIF_{abs} (maximum around 2.4 W m^{-2}) compared to over land where the maximum is ~1.5 W m^{-2} (~−35%). ΔIF_{abs} and ΔIF_{rel} are small at large CDNC because the albedo of very polluted clouds is insensitive to variations in CDNC [*Twomey*, 1991].

[34] The largest global ΔIF_{abs} (Figure 7) is found for the simulations using the DAO field, consistent with the highest $\Delta R_{eff,abs}$ of all three fields (Table 3). Global ΔIF_{abs} for GISS is about 0.03–0.05 W m^{-2} below DAO values. Although the largest ΔIF_{abs} is located in the tropics, using DAO fields tends to concentrate ΔIF_{abs} near the NH continents, whereas for simulations with GISS and FVGCM fields, ΔIF_{abs} is largest in the tropical oceans.

3.5. Sensitivity to Variation in e/e$_c$

[35] Diagnosing e implies variability in e/e_c (section 2.2), as e_c is determined by the local thermodynamic conditions (i.e., *p,T,RH*). Figure 8 (top) presents the global distribution of e/e_c for $e = 2 \times 10^{-3}$ m^{-1} (Figure 8, left) and $e = 3 \times 10^{-3}$ m^{-1} (Figure 8, right), using the GISS meteorological field; global average e/e_c is 0.34 and 0.48, respectively. In the tropics, e/e_c is considerably above the global average, approaching 0.9 for $e = 3 \times 10^{-3}$ m^{-1}, explained by the high T of these regions, resulting in lower e_c than in the midlatitudes (equation (2)). Thus CDNC in the tropics may be more susceptible to neglecting entrainment effects on droplet activation than implied in the simulations with constant e/e_c. This is reflected in ΔCDNC$_{rel}$ (Figure 8) which ranges between −13% and −20%, slightly above those obtained using fixed e/e_c (Figure 3 and Table 3). However, ΔCDNC$_{rel}$ is much larger around the tropics, being as much as −70%. This is translated into a mean $\Delta R_{eff,abs}$ about 0.1 μm larger than in the simulations assuming constant e/e_c (Table 3). In the tropics, $\Delta R_{eff,abs}$ can be as high as 3.0 μm (Figure 8). Similarly, global mean $Q_{aut}/Q_{aut,ad}$ is between 1.2 and 1.7, but can be higher (particularly in Central America and southern Africa). The pattern in IF is also substantially affected. ΔIF_{abs} (0.23 to 0.40 W m^{-2}, Table 3) is globally about 0.1 W m^{-2} greater than assuming a prescribed e/e_c. This increase results mainly from ΔIF_{abs} in the tropics, which can be as high as 3.5 W m^{-2} (Figure 8).

[36] The reduction in CDNC and increase in R_{eff} leeward of the continents is particularly important near the west coastal regions of North America, North Africa, and India (also evident in Figure 3) consistent with the CNDC and R_{eff} patterns typically observed in satellite retrievals [e.g., *Bennartz* 2007]. This is further analyzed in Figure 9 where the annual mean R_{eff} using the GISS meteorological field is compared against the average R_{eff} from MODIS retrievals for the years 2000–2006 [*King et al.*, 2006]. Compared to satellite retrievals, GMI underestimates R_{eff} by about 3–4 μm which is explained by the higher sensitivity of the retrieval to cloud top than to cloud base properties [*Chang and Li*, 2002]. Using diabatic activation reduces the difference between GMI and MODIS by about 1 μm. Qualitatively, diabatic activation results in a global pattern of R_{eff} in better agreement with MODIS, than when adiabaticity is assumed. This is particularly noticeable in the remote ocean regions of the tropics (0 to 30°S) for $e = 3 \times 10^{-3}$ m^{-1}, where regions of large R_{eff} across the tropical oceans are much better captured by GMI. The contrast in R_{eff} between land and ocean in the midlatitudes is also better represented using diabatic activation ($e = 2 \times 10^{-3}$), particularly off the West Coast of North America, and in the east coast of Africa and South America.

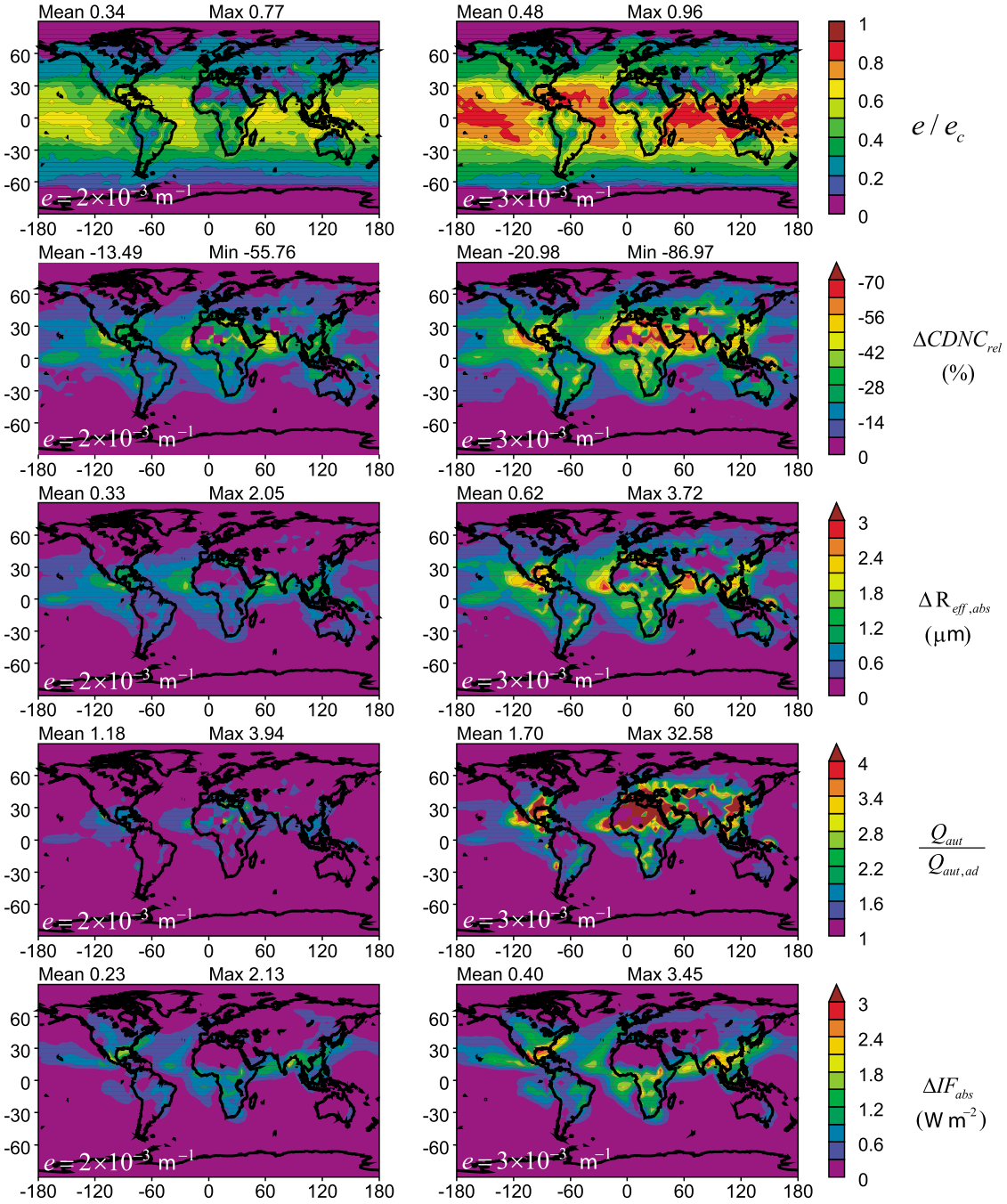

Figure 8. Annual global distribution of e/e_c, $\Delta CDNC_{rel}$, $\Delta R_{eff,abs}$, $\frac{Q_{aut}}{Q_{aut,ad}}$, and ΔIF_{abs} for $e = 2 \times 10^{-3}$ (left) m^{-1} and (right) $e = 3 \times 10^{-3}$ m^{-1}, using GISS meteorology.

The characteristic e for diabatic droplet activation may depend on the local wind dynamics [*Siebesma and Cuijpers*, 1995]. Figure 9, however, suggests that its variation may be small over large areas of the globe.

4. Discussion and Conclusions

[37] The global distribution of CDNC, IF, R_{eff}, and Q_{aut} for diabatic droplet activation was studied with the NASA GMI model using three different meteorological fields. In general, considering diabatic activation resulted in lower CDNC than when adiabatic activation was assumed. The largest variability in CDNC (up to −75%) was found in the tropics and in zones of moderate CCN concentration. The redistribution of LWC into a lower diabatic CDNC resulted in global mean R_{eff} between 0.2–0.5 μm (and locally up to 3.5 μm over the tropical oceans) higher than for adiabatic activation. Similarly, the global mean Q_{aut} is increased by a factor of 1.1 to 1.7, and as high as a factor of 4 in the tropics. It was found that by assuming adiabatic activation,

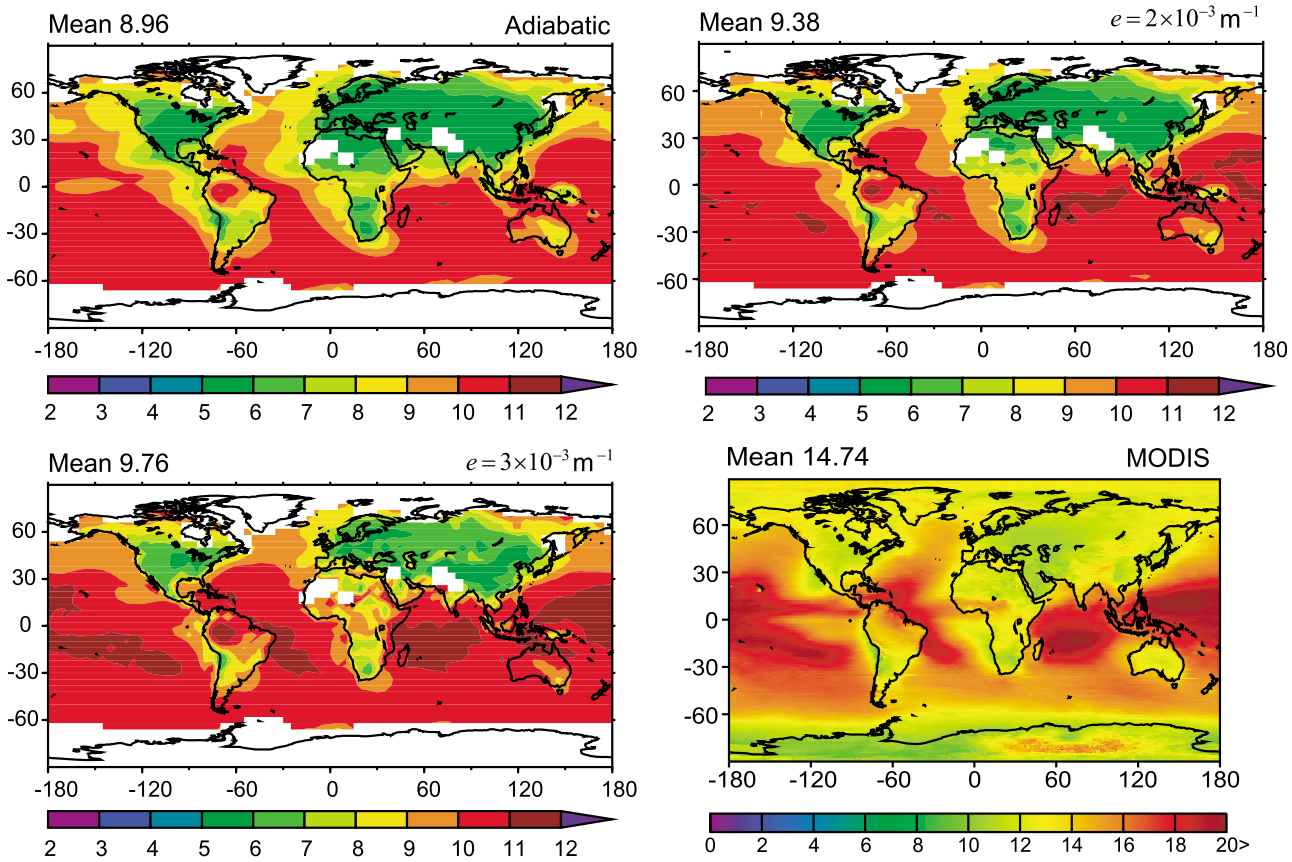

Figure 9. Annual global distribution of R_{eff} (μm) calculated using the GISS meteorology. Also shown are R_{eff} retrievals from the NASA MODIS platform averaged over the years 2000 to 2006 [*Meskhidze et al.*, 2007; *King et al.*, 2006].

IF may be overestimated between 15 and 40%. Entrainment effects on droplet activation and indirect forcing were more significant using the DAO meteorological field as $\Delta R_{eff,abs}$ was typically higher for these simulations, which is linked to the higher LWC in tropical clouds predicted by these field than with FVGCM and GISS.

[38] It was shown that areas with moderate CCN concentration (i.e., activated fraction between 0.2 and 0.5) are most prone to entrainment effects during activation (and therefore may produce a larger bias in R_{eff} when adiabatic CDNC is assumed) as the CCN spectrum is at its steepest, and CDNC most sensitive to variations in $s_{\max}$. Using adiabaticity as a proxy for e/e_c assures that our approach is consistent with current observations of the entrainment effect on LWC [e.g., *Lu et al.*, 2008; *Kim et al.*, 2008; Morales et al., submitted manuscript, 2010]. However, since e/e_c may vary throughout the globe, we considered simulations for which e was constrained using published LES simulations and field observations. Not surprisingly, IF and CDNC can be sensitive to the value of e used. Increasing e from $e = 2 \times 10^{-3}$ m^{-1} to $e = 3 \times 10^{-3}$ m^{-1} would decrease global mean ΔCDNC_{rel} from −13% and −20% and increase the global mean ΔIF_{abs} from 0.23 to 0.40 W m^{-2}. Thus, neglecting entrainment in droplet activation parameterizations would add up to about 36% uncertainty to estimations of the aerosol indirect effect. As e can vary between $e = 0.5 \times 10^{-3}$ m^{-1} and $e = 4 \times 10^{-3}$ m^{-1} [*Siebesma and Cuijpers*, 1995; *McCarthy*, 1974; *Raga et al.*, 1990; *Gregory*, 2001; *Neggers et al.*, 2003], variations in the parameter could impact IF assessments (e.g., $e = 4 \times 10^{-3}$ results in about 50% lower IF than for adiabatic activation). Hence entrainment effects on droplet activation (particularly in the tropics) may need to be considered in GCM studies.

[39] The contrast in CDNC and R_{eff} between continental and marine environments found in satellite retrievals [e.g., *Bennartz* 2007] is much better captured when diabatic (Figures 3 and 9) rather than adiabatic (Figure 2) activation is assumed. Using diabatic activation substantially improved the prediction of R_{eff} when compared to satellite retrievals, particularly in marine environments where the effect of entrainment on CDNC was the strongest (Figure 9). It is remarkable that the simple entrainment correction presented in equation (1) resulted in such an important improvement on the global pattern of R_{eff} predicted by GMI.

[40] Although this study is focused on the study of the first indirect effect, the impact of diabatic activation on Q_{aut} suggests that the cloud lifetime can also be affected. The larger R_{eff} for diabatic than for adiabatic activation would in principle lead to larger precipitation rate and shorter cloud lifetime. However, this would feedback on LWC limiting Q_{aut}. Partial droplet evaporation from entrainment (not considered in this study) is also possible and would

affect the droplet size distribution and Q_{aut} [*Brenguier and Chaumat*, 2001]. Including dynamical and hydrological feedbacks from changes in the radiative balance and autoconversion can dampen (or magnify) the magnitude of CDNC responses to entrainment [*Stevens and Feingold*, 2009], and is required to assess the effect of diabatic activation on cloud lifetime. Still, the results of this study suggests that diabatic effects on droplet formation may be an important omission in global model studies of the aerosol indirect effect.

[41] In this study aerosol distributions are prescribed and scaled to aerosol constituent mass. Although this approach is known to introduce uncertainties in the predicted CCN spectrum [*Meskhidze et al.*, 2007], particularly far from sources where aging and mixing can be significant, the conclusions of the present study may not be as sensitive to them, as we are studying the relative impact of assuming adiabatic/diabatic activation on CDNC, R_{eff}, and IF. We have also favored the possibility of running a large number of cases over using a high-resolution GCM. Using a finer resolution would not change the conclusions of this study, however, may modify the absolute values of CDNC, R_{eff}, Q_{aut} and IF. All these issues are important and require the application of a fully coupled climate model with explicit aerosol microphysics, and will be addressed in future studies. Still, the magnitude and sign of $\Delta\mathrm{CDNC}_{abs}$ and $\Delta R_{eff,abs}$ found in this study point in the right direction as R_{eff} is typically underestimated and CDNC overestimated by GCMs that use adiabatic CDNC values for forcing calculations. Thus, considering diabatic activation can provide a first-order correction to CDNC calculations that lead to more realistic distributions in predicted cloud microphysical properties and in the estimation of the aerosol indirect effect.

Notation

Q_{aut},$Q_{aut,ad}$ autoconversion rate computed using diabatic and adiabatic activation, respectively.

abs, rel subscripts indicating the absolute and relative change, respectively, from adiabatic (e = 0) to diabatic activation.

CCN cloud condensation nuclei.

C_l liquid water cloud fraction (stratiform).

CN condensation nuclei.

c_p specific heat capacity of air.

e, e_{eff} effective fractional entrainment rate.

e_c critical entrainment rate.

g acceleration of gravity.

IF indirect forcing.

M_w,M_a molar masses of water and air, respectively.

p Pressure.

$p^s(T)$ saturation vapor pressure of water.

q_l liquid water mixing ratio (stratiform).

R universal gas constant.

R_{eff} cloud droplet effective radius.

RH ambient relative humidity.

s water vapor supersaturation.

s_{max} maximum water vapor supersaturation in a cloud parcel.

T cloud parcel temperature.

t time.

T' ambient temperature.

V updraft velocity.

W liquid water mixing ratio.

α $\frac{g\Delta H_v M_w}{c_p RT^2} - \frac{gM_a}{RT}$.

γ $\frac{pM_a}{p^s(T)M_w} + \frac{M_w \Delta H_v^2}{c_p RT^2}$.

ΔH_v enthalpy of evaporation for water.

[42] **Acknowledgments.** This study was supported by NASA MAP and a NASA New Investigator Award.

References

Abdul-Razzak, H., and S. Ghan (2000), A parameterization of aerosol activation: 2. Multiple aerosol types, *J. Geophys. Res.*, *105*, 6837–6844, doi:10.1029/1999JD901161.

Abdul-Razzak, H., and S. Ghan (2005), Influence of slightly soluble organics on aerosol activation, *J. Geophys. Res.*, *110*, D06206, doi:10.1029/2004JD005324.

Albrecht, B. A., C. S. Bretherton, D. Johnson, W. H. Scubert, and A. S. Frisch (1995), The Atlantic stratocumulus transition experiment ASTEX, *Bull. Am. Meteorol. Soc.*, *76*, 889–904.

Asa-Awuku, A., and A. Nenes (2007), Effect of solute dissolution kinetics on cloud droplet formation: Extended Köhler theory, *J. Geophys. Res.*, *112*, D22201, doi:10.1029/2005JD006934.

Barahona, D., and A. Nenes (2007), Parameterization of cloud droplet formation in large scale models: Including effects of entrainment, *J. Geophys. Res.*, *112*, D16206, doi:10.1029/2007JD008473.

Barahona, D., R. West, P. Stier, S. Romakkaniemi, H. Kokkola, and A. Nenes (2010), Comprehensively accounting for the effect of giant CCN in cloud droplet activation parameterizations, *Atmos. Chem. Phys.*, *10*, 2467–2473.

Bennartz, R. (2007), Global assessment of marine boundary layer cloud droplet number, *J. Geophys. Res.*, *112*, D02201, doi:10.1029/2006JD007547.

Bloom, S., et al. (2005), Documentation and validation of the Goddard Earth Observing System (GEOS) data assimilation system: Version 4, *NASA/TM2005104606*, vol. 26, 187 pp.

Brenguier, J., and L. Chaumat (2001), Droplet spectra broadening in cumulus clouds. Part I: Broadening in adiabatic cores, *J. Atmos. Sci.*, *58*, 628–641.

Bretherton, C. S., and R. Pincus (1995), Cloudiness and marine boundary layer dynamics in the ASTEX Lagrangian experiments. Part I: Synoptic setting and vertical structure, *J. Atmos. Sci.*, *52*, 2707–2723.

Bretherton, C. S., T. Uttal, C. W. Fairall, S. E. Yuter, R. A. Weller, D. Baumgardner, K. Comstock, R. Wood, and G. B. Raga (2004), The epic 2001 stratocumulus study, *Bull. Am. Meteorol. Soc.*, *85*, 967–977.

Carpenter, R., K. Droegemeier, and A. Blyth (1998), Entrainment and detrainment in numerically simulated cumulus congestus clouds. Part I: General results, *J. Atmos. Sci.*, *55*, 3417–3432.

Chang, F.-L., and Z. Li (2002), Estimating the vertical variation of cloud droplet effective radius using multispectral near-infrared satellite measurements, *J. Geophys. Res.*, *107*(D15), 4257, doi:10.1029/2001JD000766.

Chen, W., A. Nenes, H. Liao, P. Adams, J. Li, and J. Seinfeld (2010), Global climate response to anthropogenic aerosol indirect effects: Present day and year 2100, *J. Geophys. Res.*, *115*, D12207, doi:10.1029/2008JD011619.

Chosson, F., J. Brenguier, and L. Schüller (2007), Entrainment-mixing and radiative transfer simulation in boundary layer clouds, *J. Atmos. Sci.*, *64*, 2670–2682.

Chou, M.-D., M. Suarez, C.-H. Ho, M.-H. Yan, and K.-T. Lee (1998), Parameterizations for cloud overlapping and shortwave single-scattering properties for use in general circulation and cloud ensemble models, *J. Clim.*, *11*, 202–214.

Cohen, C. (2000), A quantitative investigation of entrainment and detrainment in numerically simulated cumulonimbus clouds, *J. Atmos. Sci.*, *57*, 1657–1674.

Conant, W. C., et al. (2004), Aerosol-cloud drop concentration closure in warm clouds, *J. Geophys. Res.*, *109*, D13204, doi:10.1029/2003JD004324.

Del Genio, A., M. Yao, W. Kovari, and K. Lo (1996), A prognostic cloud water parameterization for global climate models, *J. Clim.*, *9*, 270–304.

Dong, X., T. P. Ackerman, E. E. Clothiaux, P. Pilewskie, and Y. Han (1997), Microphysical and radiative properties of boundary layer stratiform clouds deduced from ground-based measurements, *J. Geophys. Res.*, *102*, 23,829–23,843.

Donner, L. J., C. J. Seman, R. S. Hemler, and S. Fan (2001), A cumulus parameterization including mass fluxes, convective vertical velocities, and mesoscale effects: Thermodynamic and hydrological aspects in a general circulation model, *J. Clim.*, *14*, 3444–3463.

Feingold, G., I. Koren, H. Wang, H. Xue, and W. Brewer (2010), Precipitation-generated oscillations in open cellular cloud fields, *Nature*, *466*, 849–852.

Feng, Y., J. Penner, S. Sillman, and X. Liu (2004), Effects of cloud overlap in photochemical models, *J. Geophys. Res.*, *109*, D04310, doi:10.1029/2003JD004040.

Fountoukis, C., and A. Nenes (2005), Continued development of a cloud droplet formation parameterization for global climate models, *J. Geophys. Res.*, *110*, D11212, doi:10.1029/2004JD005591.

Fountoukis, C., et al. (2007), Aerosol-cloud drop concentration closure for clouds sampled during the International Consortium for Atmospheric Reseach on Transport and Transformation 2004 campaign, *J. Geophys. Res.*, *112*, D10S30, doi:10.1029/2006JD007272.

Gerber, H., G. Frick, S. Malinowski, J.-L. Brenguier, and F. Burnet (2005), Holes and entrainment in stratocumulus, *J. Atmos. Sci.*, *62*, 443–459.

Ghan, S., L. Leung, R. Easter, and H. Abdul-Razzak (1997), Prediction of cloud droplet number in a general circulation model, *J. Geophys. Res.*, *102*, 21,777–21,794.

Grabowski, W., and H. Pawlowska (1993), Entrainment and mixing in clouds: The Paluch diagram revisited, *J. Appl. Meteorol.*, *32*, 1767–1773.

Gregory, D. (2001), Estimation of entrainment rate in simple models of convective clouds, *Q. J. R. Meteorol. Soc.*, *127*, 53–72.

Guibert, S., J. Snider, and J. Brenguier (2003), Aerosol activation in marine stratocumulus clouds: 1. Measurement validation for a closure study, *J. Geophys. Res.*, *108*(D15), 8628, doi:10.1029/2002JD002678.

Hack, J. (1998), Sensitivity of the simulated climate to a diagnostic formulation for cloud liquid water, *J. Clim.*, *11*, 1497–1515.

Hsieh, W., G. Buzorius, R. Flagan, J. H. Seinfeld, and A. Nenes (2009a), On the representation of droplet coalescence and autoconversion: Evaluation using ambient cloud droplet size distributions, *J. Geophys. Res.*, *114*, D07201, doi:10.1029/2008JD010502.

Hsieh, W., H. Jonsson, G. Buzorius, R. Flagan, J. H. Seinfeld, and A. Nenes (2009b), Parameterization of cloud drop size distribution in regional and large scale models, *J. Geophys. Res.*, *114*, D11205, doi:10.1029/2008JD011387.

Jiang, H., H. Xue, A. Teller, G. Feingold, and Z. Levin (2006), Aerosol effects on the lifetime of shallow cumulus, *Geophys. Res. Lett.*, *33*, L14806, doi:10.1029/2006GL026024.

Kain, J., and J. M. Fritsch (1990), A one-dimensional entraining/detraining plume model and its application in convective parameterization, *J. Atmos. Sci.*, *47*, 2784–2802.

Khairoutdinov, M., and Y. Kogan (2000), A new cloud physics parameterization in a large-eddy simulation model of marine stratocumulus, *Mon. Weather Rev.*, *128*, 229–243.

Kiehl, J. (1994), Sensitivity of a GCM climate simulation to differences in continental versus maritime cloud drop size, *J. Geophys. Res.*, *99*, 23,107–23,115.

Kim, B., M. Miller, S. Schwartz, Y. Liu, and Q. Min (2008), The role of adiabaticity in the aerosol first indirect effect, *J. Geophys. Res.*, *113*, D05210, doi:10.1029/2007JD008961.

King, M., S. Platnick, P. A. Hubanks, G. T. Arnold, E. G. Moody, G. Wind, and B. Wind (2006), Collection 005 change summary for the MODIS cloud optical property (06-OD) algorithm, http://modis-atmos.gsfc.nasa.gov, p. 101, NASA Goddard Space Flight Cent., Greenbelt, Md.

Korolev, A. V. (1995), The influence of supersaturation fluctuations on droplet size spectra formation, *J. Atmos. Sci.*, *52*, 3620–3634.

Kumar, P., I. N. Sokolik, and A. Nenes (2009), Parameterization of cloud droplet formation for global and regional models: Including adsorption activation from insoluble CCN, *Atmos. Chem. Phys.*, *9*, 2517–2532.

Lance, S., A. Nenes, and T. Rissman (2004), Chemical and dynamical effects on cloud droplet number: Implication for estimates of the aerosol indirect effect, *J. Geophys. Res.*, *109*, D22208, doi:10.1029/2004JD004596.

Lin, C., and A. Arakawa (1997), The macroscopic entrainment processes of simulated cumulus ensemble. Part I: Entrainment sources, *J. Atmos. Sci.*, *54*, 1027–1043.

Liu, X., J. Penner, and M. Herzog (2005), Global modeling of aerosol dynamics: Model description, evaluation, and interactions between sulfate and nonsulfate aerosols, *J. Geophys. Res.*, *110*, D18206, doi:10.1029/2004JD005674.

Liu, X., J. Penner, B. Das, D. Bergmann, J. Rodriguez, S. Strahan, M. Wang, and Y. Feng (2007), Uncertainties in global aerosol simulations: Assessment using three meteorological data sets, *J. Geophys. Res.*, *112*, D11212, doi:10.1029/2006JD008216.

Lohmann, U., and J. Feichter (1997), Impact of sulfate aerosols on albedo and lifetime of clouds: A sensitivity study with the ECHAM4 GCM, *J. Geophys. Res.*, *102*, 13,685–13,700.

Lu, M., G. Feingold, H. Jonsson, P. Chuang, H. Gates, R. Flagan, and J. H. Seinfeld (2008), Aerosol-cloud relationships in continental shallow cumulus, *J. Geophys. Res.*, *113*, D15201, doi:10.1029/2007JD009354.

McCarthy, J. (1974), Field verification of the relationship between entrainment rate and cumulus cloud diameter, *J. Atmos. Sci.*, *31*, 1028–1039.

McFiggans, G., et al. (2005), The effect of physical and chemical aerosol properties on warm cloud droplet activation, *Atmos. Chem. Phys.*, *5*, 8507–8646.

Medina, J., A. Nenes, R. Sotiropoulou, L. Cottrell, L. Ziemba, P. Beckman, and R. Griffin (2007), Cloud condensation nuclei closure during the International Consortium for Atmospheric Research on Transport and Transformation 2004 campaign: Effects of size resolved composition, *J. Geophys. Res.*, *112*, D10S31, doi:10.1029/2006JD007588.

Meskhidze, N., A. Nenes, W. C. Conant, and J. H. Seinfeld (2005), Evaluation of a new cloud droplet activation parameterization with in situ data from CRYSTAL-FACE and CSTRIPE, *J. Geophys. Res.*, *110*, D16202, doi:10.1029/2004JD005703.

Meskhidze, N., R. E. P. Sotiropoulou, A. Nenes, J. Kouatchou, B. Das, and J. M. Rodriguez (2007), Aerosol-cloud interactions in the NASA GMI: Model development and indirect forcing assessments, *Atmos. Chem. Phys. Discuss.*, *7*, 14,295–14,330.

Ming, Y., V. Ramaswamy, L. Donner, and V. Phillips (2006), A new parameterization of cloud droplet activation applicable to general circulation models, *J. Atmos. Sci.*, *63*, 1348–1356.

Morales, R., and A. Nenes (2010), Characteristic updrafts for computing distribution-averaged cloud droplet number, and stratocumulus cloud properties, *J. Geophys. Res.*, *115*, D18220, doi:10.1029/2009JD013233.

Morrison, H., and A. Gettelman (2008), A new two-moment bulk stratiform cloud microphysics scheme in the Community Atmosphere Model, version 3 (CAM3). Part I: Description and numerical tests, *J. Clim.*, *21*, 3642–3659.

Morrison, H., and W. Grabowski (2008), Modeling supersaturation and subgrid-scale mixing with two-moment bulk warm microphysics, *J. Atmos. Sci.*, *65*, 792–812.

Morton, B., S. Taylor, and J. Turner (1956), Turbulent gravitational convection from maintained and instantaneous sources, *Proc. R. Soc. London Ser. A*, *234*, 1–23.

Neggers, R., P. Duynkerke, and M. Rodts (2003), Shallow cumulus convection: A validation of large-eddy simulation against aircraft and Landsat observations, *Q. J. R. Meteorol. Soc.*, *129*, 2671–2696.

Nenes, A., and J. H. Seinfeld (2003), Parameterization of cloud droplet formation in global climate models, *J. Geophys. Res.*, *108*(D14), 4415, doi:10.1029/2002JD002911.

Nenes, A., R. Charlson, M. Facchini, M. Kulmala, A. Laaksonen, and J. H. Seinfeld (2002), Can chemical effects on cloud droplet number rival the first indirect effect?, *Geophys. Res. Lett.*, *29*(17), 1848, doi:10.1029/2002GL015295.

Paluch, I. (1979), The entrainment mechanism in Colorado cumuli, *J. Atmos. Sci.*, *36*, 2467–2478.

Peng, Y., U. Lohmann, and W. Leaitch (2005), Importance of vertical velocity variations in the cloud droplet nucleation process of marine stratocumulus, *J. Geophys. Res.*, *110*, D21213, doi:10.1029/2004JD004922.

Pruppacher, H., and J. Klett (1997), *Microphysics of Clouds and Precipitation*, 2nd ed., Kluwer Acad., Boston.

Pruppacher, H., and I. Lee (1976), A comparative study of the growth of cloud drops by condensation using an air parcel model with and without entrainment, *Pure Appl. Geophys.*, *115*, 523–545.

Quaas, J., et al. (2009), Aerosol indirect effects: General circulation model intercomparison and evaluation with satellite data, *Atmos. Chem. Phys.*, *9*, 8697–8717.

Raga, G., and P. Jonas (1993), On the link between cloud-top radiative properties and sub-cloud aerosol concentrations, *Q. J. R. Meteorol. Soc.*, *119*, 1419–1425.

Raga, G., J. Jensen, and M. Baker (1990), Characteristics of cumulus band clouds off the coast of Hawaii, *J. Atmos. Sci.*, *47*, 338–335.

Randall, D., M. Khairoutdinov, A. Arakawa, and W. Grabowski (2003), Breaking the parameterization deadlock, *Bull. Am. Meteorol. Soc.*, *84*, 1547–1564.

Rogers, D., J. Telford, and S. Chai (1985), Entrainment and the temporal development of the microphysics of convective clouds, *J. Atmos. Sci.*, *42*, 1846–1858.

Rotman, D., et al. (2001), Global modeling initiative assessment model: Model description, integration, and testing of the transport shell, *J. Geophys. Res.*, *106*, 1669–1691.

Segal, Y., and A. Khain (2006), Dependence of droplet concentration of aerosol conditions in different cloud types: Application to droplet con-

centration parameterization of aerosol conditions, *J. Geophys. Res.*, *111*, D15204, doi:10.1029/2005JD006561.
Seinfeld, J. H., and S. N. Pandis (1998), *Atmospheric Chemistry and Physics*, John Wiley, New York.
Siebesma, A., and J. Cuijpers (1995), Evaluation of parametric assumptions for shallow cumulus convection, *J. Atmos. Sci.*, *52*, 650–666.
Snider, J., S. Guibert, J. Brenguier, and J.-P. Putaud (2003), Aerosol activation in marine stratocumulus clouds: 2. Kohler and parcel theory closure studies, *J. Geophys. Res.*, *108*(D15), 8629, doi:10.1029/2002JD002692.
Stevens, B. (2005), Atmospheric moist convection, *Annu. Rev. Earth Planet. Sci.*, *33*, 605–643.
Stevens, B., and G. Feingold (2009), Untangling aerosol effects on clouds and precipitation in a buffered system, *Nature*, *461*, 607–613.
Stommel, H. (1947), Entrainment of air into a cumulus cloud, *J. Meteorol.*, *4*, 91–94.
Takemura, T., T. Nozawa, S. Emori, T. Y. Nakajima, and T. Nakajima (2005), Simulation of climate response to aerosol direct and indirect effects with aerosol transport-radiation model, *J. Geophys. Res.*, *110*, D02202, doi:10.1029/2004JD005029.
Twomey, S. (1977), The influence of pollution on the shortwave cloud albedo of clouds, *J. Atmos. Sci.*, *34*, 1149–1152.
Twomey, S. (1991), Aerosols, clouds and radiation, *Atmos. Environ., Part A*, *25*, 2435–2442.
Wang, Q., and B. Albrecht (1994), Observations of cloud-top entrainment in marine stratocumulus clouds, *J. Atmos. Sci.*, *51*, 1530–1547.
Wood, R. (2007), Cancellation of aerosol indirect effects in marine stratocumulus through cloud thinning, *J. Atmos. Sci.*, *64*, 2657–2669.
Xu, K., and S. Krueger (1991), Evaluation of cloudiness parameterizations using a cumulus ensemble model, *Mon. Weather Rev.*, *119*, 342–367.

D. Barahona, Global Modeling and Assimilation Office, Code 610.1, NASA Goddard Space Flight Center, Greenbelt, MD 20771, USA.
A. Nenes, School of Earth and Atmospheric Sciences, Georgia Institute of Technology, 331 Ferst Dr., Atlanta, GA 30332-0340, USA. (athanasios.nenes@gatech.edu)
R. Sotiropoulou, Environmental Research Laboratory, INT-RP, N.C.S.R. Demokritos, Aghia Paraskevi, 15310, Greece.